DOI: 10.1002/chem.200500516

Ligand-Gated Synthetic Ion Channels

Pinaki Talukdar, Guillaume Bollot, Jiri Mareda, Naomi Sakai, and Stefan Matile*[a]

Abstract: Supramolecular π-stack architecture is fundamental in DNA chemistry but absent in biological and synthetic ion channels and pores. Here, a novel rigid-rod π-stack architecture is introduced to create synthetic ion channels with characteristics that are at the forefront of rational design, that is, ligand gating by a conformational change of the functional supramolecule. Namely, the intercalation of electron-rich aromatics is designed to untwist inactive electron-poor helical π-stacks without internal space into open barrel-stave ion channels. Conductance experiments in planar lipid bilayers corroborate results from spherical bilayers and molecular modeling: Highly cooperative and highly selective ligand gating produces small, long-lived, weakly anion selective, ohmic ion channels. Structural studies conducted under conditions relevant for function provide experimental support for helix–barrel transition as origin of ligand gating. Control experiments demonstrate that minor structural changes leading to internal decrowding suffice to cleanly annihilate chiral self-organization and function.

Keywords: bioorganic chemistry · ion channels · pi interactions · self-assembly · supramolecular chemistry

Introduction

After the creation of unifunctional ion channels as such,[1] scientific attention is continuously shifting toward "smart" supramolecular architecture with refined, multiple functions.[2–19] Early breakthroughs on the recognition of non-trivial ions[2] and specific characteristics of lipid bilayer membranes such as polarization[3] were followed by many remarkable studies on ion and membrane selectivity. The more recent combination of molecular translocation with molecular recognition[4] and transformation[5] lead to the concept of synthetic multifunctional pores and practical applications[6,7] in sensing and catalysis.[8–10] Current research on molecular recognition by not only synthetic[1–19] but also bioengineered[20,21] and biological[22] ion channels and pores as sensors focuses, however, almost exclusively on blockage.

The more demanding pore opening in response to molecular recognition was achieved last year with a synthetic multifunctional pore from the classical rigid-rod β-barrel series.[7] External pore design focusing on the modulation of pore–membrane interactions resulted in pore activation in response to chemical stimulation that could be used for the continuous detection of chemical reactions. This synergism was further proven on the structural level to originate from ligand-mediated change in partitioning, presumably without conformational change of the pore. Indeed, we failed so far to find a strategy that would produce closed rigid-rod β-barrel architecture without internal space which could physically open up by a conformational change in response to chemical stimulation. Therefore, replacement of the β-sheet hoops in rigid-rod β-barrels by π-stacks appeared as a choice. In the resulting "π-barrel," the repeat distance of 4.9 Å of the *p*-octophenyl stave should exceed the repeat distance of around 3.4 Å between "π-hoops" (Figure 1). Therefore, a rigid-rod π-barrel should twist into a rigid-rod "π-helix" with matched hoop-stave repeats (e.g. $\mathbf{1}^{nH}$, Figure 1). Such a notional rigid-rod π-helix was envisioned as the desired closed ion channel where aromatic ligands could intercalate, initiate the untwisting helix–barrel transition and give an open barrel-stave ion channel (e.g. $\mathbf{1}^{n}\cdot\mathbf{2}^{m}$, Figure 1).

The envisioned π-stack architecture and intercalation chemistry is reminiscent of chemistry and biology of oligonucleotides such as DNA duplexes, but rare, if not unknown as architecture of biological or synthetic ion channels and pores.[1–22] The compatibility of π-stack architecture with the cylindrical interface between aqueous interior and non-polar surrounding of ion channels and pores was unknown and

[a] P. Talukdar, G. Bollot, Dr. J. Mareda, Dr. N. Sakai, Prof. S. Matile
Department of Organic Chemistry, University of Geneva
Geneva (Switzerland)
Fax: (+41) 22-379-3215
E-mail: stefan.matile@chiorg.unige.ch

Supporting information for this article is available on the WWW under http://www.chemeurj.org/ or from the author: Experimental Section.

therefore reason for concern. However, due to remarkable progress in supramolecular chemistry, a marvelous collection of π-stack architectonics was on hand to address these questions. One of the best-explored motifs is the purple charge-transfer (CT) complex formed by dialkoxynaphthalene (DAN) donors and naphthalenediimide (NDI) acceptors. These complexes have already been of use to create single- and double-stranded oligo-DAN–NDI foldamers,[23–25] switchable DAN–NDI rotaxanes[26,27] and DAN–NDI catenanes.[28–30]

Encouraged by these spectacular applications to refined architecture, we decided to use the DAN–NDI motif for the creation of ligand-gated synthetic ion channels. The electron-poor NDI acceptors rather than electron-rich DAN donors were used in the envisioned π-stack architecture because of their preference for face-to-face self-assembly.[31] The *p*-octiphenyls **1** with eight NDIs along the rigid-rod scaffold were expected to self-assemble into π-helices $\mathbf{1}^{nH}$. Helix–barrel transition in response to the intercalation of DAN donors **2** should then give open ion channel $\mathbf{1}^{n}\cdot\mathbf{2}^{m}$. Ligand **2** was equipped with an anionic tail on one and an alkyl tail on the other side to support CT complex formation by ion pairing within the cationic interior of the notional π-barrel $\mathbf{1}^{n}\cdot\mathbf{2}^{m}$ and external hydrophobic contacts with the surrounding bilayer membrane, respectively (Figure 1B).

Four additional design principles were applied to assure the formation of rigid-rod π-stack architecture of $\mathbf{1}^{nH}$ and $\mathbf{1}^{n}\cdot\mathbf{2}^{m}$ despite the poor directionality of aromatic interactions between the intercalating NDI hoops and in DAN–NDI CT complexes.

1) To promote self-assembly into cylindrical supramolecular oligomers (and to prevent linear self-assembly into supramolecular polymers), it was important to place corners in the suprastructure. Rigid *p*-octiphenyl rods with seven adaptable, chiral biphenyl torsion angles $\omega \neq 0$ per stave are considered to be perfect for this purpose.[8,9]
2) Amides were installed at both ends of the NDI to form hydrogen-bonded chains along the NDI stacks oriented parallel to the rigid-rod staves (Figure 1A). These hydrogen-bonded chains were expected to position the π-stacks like hoops in the barrel-stave architecture.[32–34] In geometry-minimized molecular models, these hydrogen-bonded chains were intact after the intercalation of DAN ligands. In hydrophobic bilayer membranes, the hydrophilic alkylammonium tails consequently point toward the interior of the barrel (Figure 1A).
3) Internal crowding[8,9] was expected to promote the self-assembly of higher hollow oligomers by steric hindrance between bulk at the inner surface (and to prevent the self-assembly of dimers without internal space). Internal crowding was introduced with the alkylammonium tails; variation of their length should vary the magnitude of internal crowding (see below for experimental support).

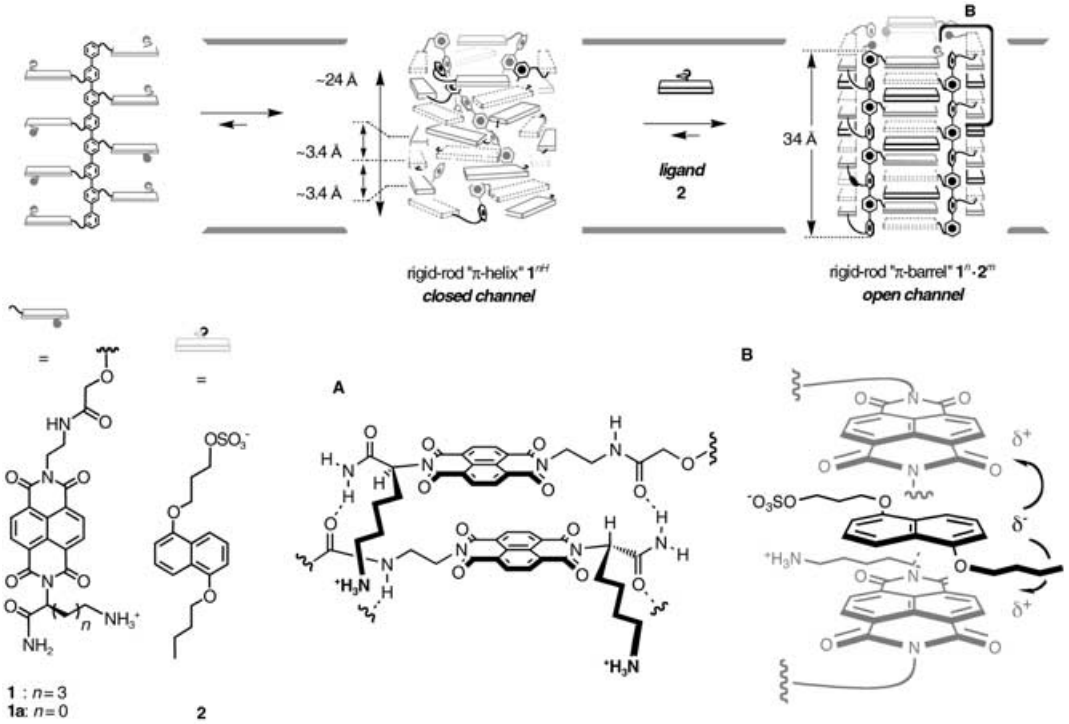

Figure 1. Ligand-gated opening of notional rigid-rod π-helix $\mathbf{1}^{nH}$ into ion channel $\mathbf{1}^{n}\cdot\mathbf{2}^{m}$ by intercalation of DAN ligands **2** with magnified views of A) an NDI–NDI stack to illustrate internal crowding, internal charge repulsion and flanking H-bonded chains, and B) an NDI–DAN–NDI CT complex. All suprastructures are simplifications that are, however, consistent with experimental data and molecular models (Figure 3); stoichiometries of supramolecules are unknown.

4) According to the ICR model,[35] internal charge repulsion is another key parameter to promote the self-assembly of higher hollow oligomers like barrel-stave supramolecules.[8,9] Intermediate internal charge repulsion, dependent on proximity effects, pH and ionic strength, was taken care of by the partially deprotonated[35] alkylammonium tails as well.

In the following, we first use conductance measurements in planar lipid bilayers to characterize single ligand-gated ion channels $\mathbf{1}^n\cdot\mathbf{2}^m$ as small, long-lived, weakly anion selective and ohmic. The characteristics found are in good agreement with those from functional studies in vesicles described in the preliminary communication on this topic.[36] We then continue with structural studies in support of a conformational change of the rigid-rod π-stack architecture, that is the helix–barrel transition from $\mathbf{1}^{nH}$ to $\mathbf{1}^n\cdot\mathbf{2}^m$, as origin of ligand gating to finish up with a study on internal decrowding, demonstrating that a remarkably minor change in monomer structure suffices to cleanly annihilate all supramolecular architecture and function.

A brief comment concerning the term "ligand gating" may be appropriate to avoid eventual misunderstandings. The use of this term with regard to function (i.e., ligand-mediated increase in "channel activity") appears to be unproblematic in the context of this study. The specific structural implications often associated with "ligand gating" (i.e., ligand-mediated changes in channel conformation) are evaluated in this study and shown to apply within reason. Differences to "biological ligand gating" beyond completely abiotic architecture and gating mechanism include the use of more than one ligand to open the channel. Moreover, the enzyme-regulated reversibility of "biological ligand gating," although in principle unproblematic,[8] has so far not been studied experimentally.

Results and Discussion

The synthesis of the target molecule **1** from commercial starting materials in overall 13 steps has been communicated.[36] Initially, ligand gating was determined in spherical egg yolk phosphatidylchline (EYPC) bilayers (i.e., large unilamellar vesicles, LUVs) by using the HPTS assay. According to the HPTS assay, the opening of the poorly active π-helices $\mathbf{1}^{nH}$ by ligand **2** occurs in a highly cooperative manner ($n=6.5$) at an effective concentration $EC_{50}=13.7$ μM. Negligible activity found with DAN controls lacking either the anionic or the hydrophobic tail as well as intercalators such as AMP or GMP indicated that ligand-gated formation of ion channels $\mathbf{1}^n\cdot\mathbf{2}^m$ is highly selective. Inability to mediate the efflux of large organic anions and cations indicated that ion channels $\mathbf{1}^n\cdot\mathbf{2}^m$ are small. Competition experiments revealed that, according to the HPTS assay, ion channels $\mathbf{1}^n\cdot\mathbf{2}^m$ are anion selective with an inhibition sequence $SO_4^{2-} > NO_3^- \approx I^- > Cl^- \approx Br^- > AcO^- > F^-$. These results from the HPTS assay in vesicles have already been described in the preliminary communication on this topic.[36]

Single-channel conductance: In planar EYPC membranes, single-channel currents could be observed only when rod **1** and ligand **2** were added together (Figure 2). The presence of several conducting states was consistent with the supramolecular nature of ion channels $\mathbf{1}^n\cdot\mathbf{2}^m$. Considering the suprastructural complexity of the challenged synergism, the found single-current levels were surprising homogeneous and inert. The most frequently observed single channels were long-lived (Figure 2C) and ohmic (Figure 2D). The reversal potential $V_r=+4.6$ mV found at a 2.0 M → 0.5 M KCl gradient gave the permeability ratio $P_{Cl^-}/P_{K^+}=1.38$. This weak anion selectivity was in agreement with the selectivity of ligand-gated ion channels $\mathbf{1}^n\cdot\mathbf{2}^m$ determined with the HPTS assay in spherical EYPC membranes.

The two frequently observed single-channel conductances showed ohmic behavior (Figure 2D). The inner diameter of the ligand-gated ion channel $\mathbf{1}^n\cdot\mathbf{2}^m$ was calculated from the dominant single-channel conductance $g=94$ pS using the Hille equation with Sansom's correction factor of 5.61.[37,38] A corrected[38] inner channel diameter $d=3.5$ Å was obtained. This value was in agreement with the inner diameters of geometry-minimized molecular models of ligand-gated ion channels $\mathbf{1}^n\cdot\mathbf{2}^m$ with about twelve ($\mathbf{1}^4\cdot\mathbf{2}^{12}$, $d=5.4$ Å) to sixteen ligands per tetramer ($\mathbf{1}^4\cdot\mathbf{2}^{16}$, $d=3.0$ Å, Figure 3B). Moreover, the inner diameter $d=3.5$ Å of ligand-gated ion channels $\mathbf{1}^n\cdot\mathbf{2}^m$ calculated from the single-channel conductance in planar bilayers was in excellent agreement with size-exclusion experiments in vesicles.

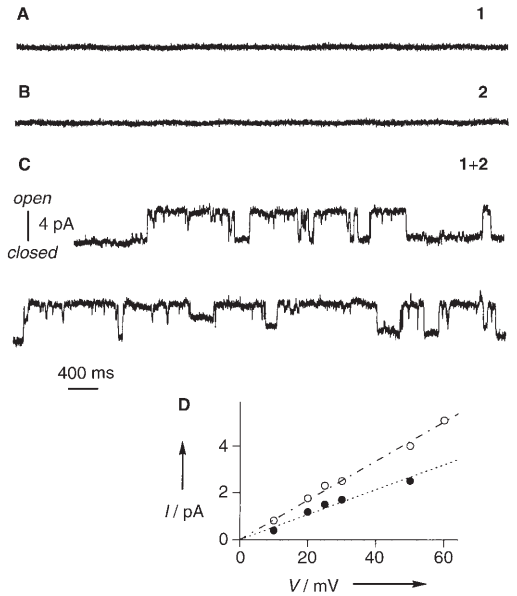

Figure 2. Planar EYPC bilayer conductance in the presence of A) **1** (5 μM *cis*), B) **2** (2.4 μM *cis*) and C) **1** (5 μM *cis*) and **2** (2.4 μM *cis*) at +50 mV (*trans* at ground) in 2 M KCl. D) IV profile of two different frequent single-channel current levels (open and closed circles) with linear curve fit.

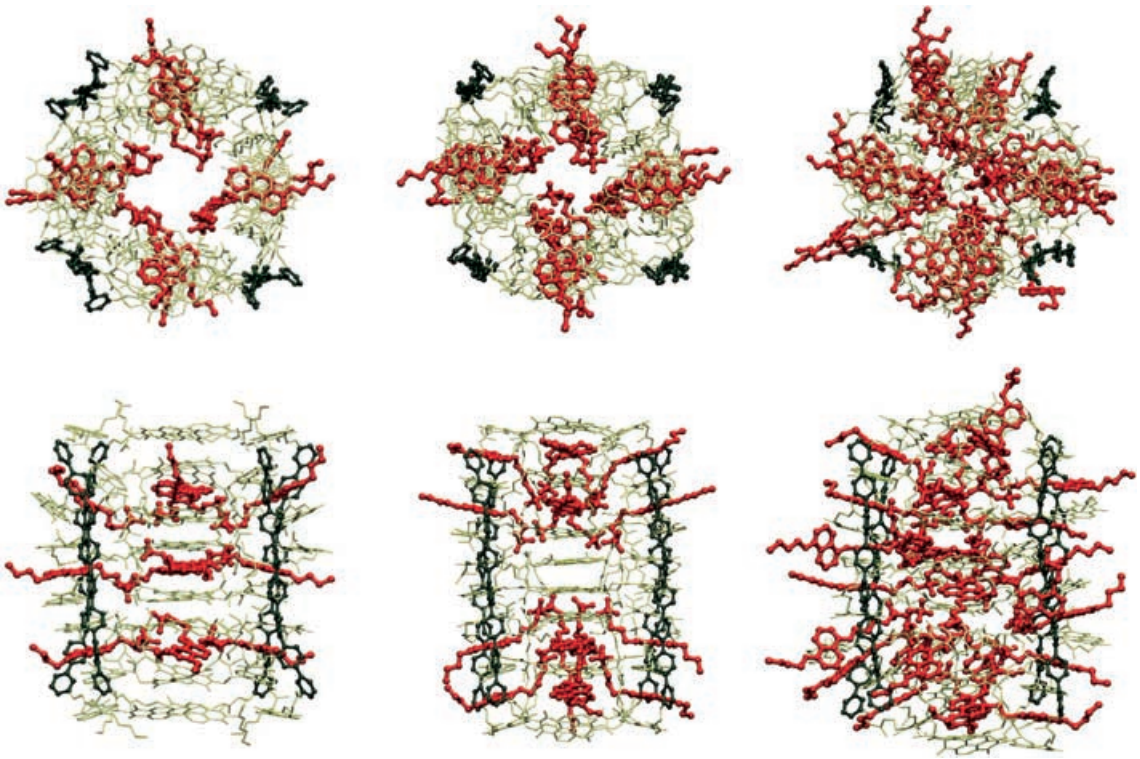

Figure 3. Optimized geometry of molecular models of complexes $\mathbf{1}^{4}\cdot\mathbf{2}^{12}$ (left, barrel length $l=38$ Å, inner diameter $d=5.4$ Å), $\mathbf{1}^{4}\cdot\mathbf{2}^{16}$ (middle, $l=42$ Å, $d=3.0$ Å) and $\mathbf{1}^{4}\cdot\mathbf{2}^{28}$ (right, $l=45$ Å, $d=2.0$ Å) in side (bottom) and axial view (top). *p*-Octiphenyl staves (dark green) and DAN ligands (red) are both in ball-and-stick representation, NDI hoops (light green) are in wire representation, H omitted, 50% (left) to 100% (middle, right) amine protonation, 0% sulfate protonation ($\mathbf{1}^{4}\cdot\mathbf{2}^{12}$ is adapted from[36] with permission, Copyright 2005 Am. Chem. Soc.).

Structural studies: To minimize the probability to produce irrelevant, misleading findings, structural studies were strictly limited to conditions relevant for function, that is, complexes $\mathbf{1}^{n}\cdot\mathbf{2}^{m}$ at low micromolar concentrations in the presence of EYPC bilayer membranes.[8,9] Fluorescence and circular dichroism (CD) spectroscopy were compatible with these restrictive conditions. The NDI chromophore[39] of channel $\mathbf{1}^{n}$ and the DAN fluorophore[40] of ligand **2** were available as intrinsic probes. The otherwise invaluable blue emission of the *p*-octiphenyl stave[7–9] was completely quenched by the NDI hoops.

The interaction of ligand **2** with lipid-bilayer membranes was studied first (Figure 4). In the absence of rod **1**, ligand **2** exhibited increasing excimer emission[40] with increasing membrane concentration. Conventional data treatment[41] gave a partition coefficient $K_x = 8.0 \pm 0.6\times10^{5}$ (Figure 4, inset). This finding suggested that ligands **2** would approach rod **1** in the membrane rather than in the water, and presumably not as monomers.

The self-organization of rod **1** in the presence and absence of lipid bilayer membranes was studied next (Figure 5). The CD spectrum of rod **1** in water and the "membrane-mimetic" 2,2,2-trifluoroethanol (TFE) exhibited a strong band-I Cotton effect with vibrational fine structure overlapping the exciton band splitting (Figure 5A, black). The observed bisignate band-I Cotton effect originates from exciton coupling of non-parallel N,N-polarized electric π–π* transitions between two NDI chromophores that are positioned close in space with a well-defined and significant twist.[39,42] The magnitude of the observed CD amplitude around $A = -24\,\mathrm{M^{-1}\,cm^{-1}}$ was comparable to that of pertinent covalent CD model compounds like the classical 1*R*,2*R*-cyclohexanediamine derivative ($A=\Delta\varepsilon_1$ (391 nm) $-$ $\Delta\varepsilon_2$ (~353 nm)).[39] This similarity to ideal covalent positioning of perfectly twisted proximal NDIs demonstrated that the self-organization of rod **1** is significant. Indeed, monomeric control **1b**

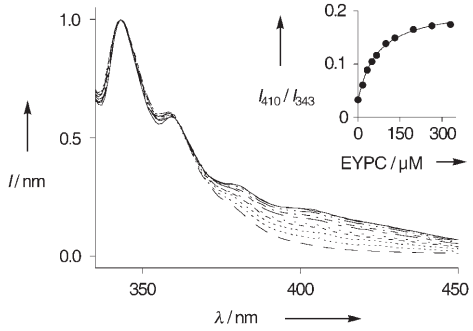

Figure 4. Emission spectra of **2** (20 μM) with increasing concentration of EYPC LUVs [0 (-----) → 330 μM EYPC (——), λ_{ex} 325 nm]. Inset: Fractional emission intensity I_{410}/I_{343} as a function of lipid concentration with curve fit to the White equation.[41]

(Figure 5A, grey) but also control rod **1a** with nearly identical monomer structure (below) were almost CD silent. The significant helical twist seen in CD spectrum of rod **1** was in excellent agreement with the notional π-helix $\mathbf{1}^{nH}$, the negative sign of the CD amplitude demonstrated *M* helicity (Figure 1).[39,42]

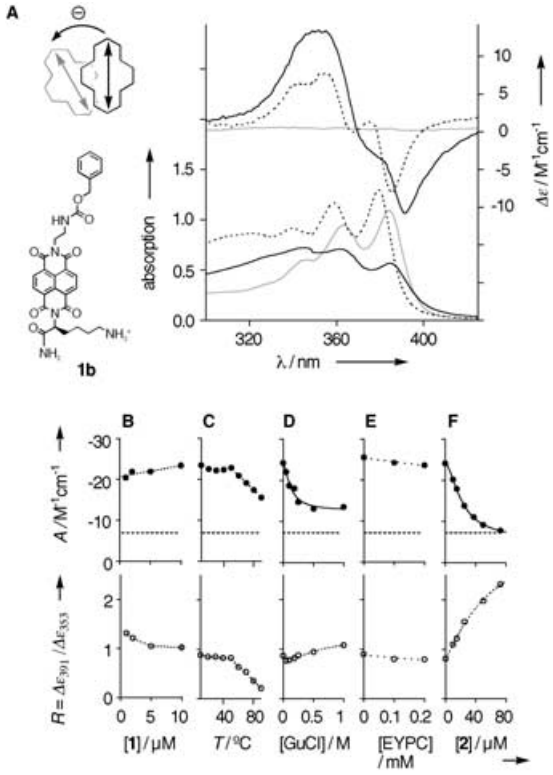

Figure 5. A) CD (top) and UV/Vis spectra (bottom) of **1** in buffer (——) and TFE (•••••) compared with monomer **1b** (50 μM, grey) with correlation of amplitude sign with the absolute sense of twist of coupled NDIs[39] and dependence of CD amplitude *A* (top) and CD ratio *R* (Δε 391 nm/Δε 353 nm, bottom) on B) the concentration of **1**; C) the temperature and the presence of increasing concentrations of D) guanidinium chloride, E) vesicles and F) ligand **2** (compare Figure 6); constants: 10 mM HEPES, 100 mM NaCl, pH 7.9, 25 °C, 200 μM EYPC (D, F). The dotted line in B–F (top) indicates the CD amplitude of complex $\mathbf{1}^{n}\cdot\mathbf{2}^{m}$ (F).

The bisignate band-I Cotton effect in the CD spectrum of rod **1** was concentration independent (Figure 5B). This finding demonstrated that the expected self-assembly into notional π-helix $\mathbf{1}^{nH}$ is exergonic and that the number of monomers per supramolecule cannot be determined from the c_M profile.[43] Thermal denaturation of notional π-helix $\mathbf{1}^{nH}$ revealed stability up to 50 °C followed by a steady decrease to $A = -16\,\mathrm{M^{-1}cm^{-1}}$ at 90 °C. Considering the possibility of incomplete denaturation near boiling, the found melting temperature was best described as $T_M \geq 70$ °C. For comparison, a DNA duplex of similar length has a $T_M = 45$ °C ($d(GT)_7$/$d(AC)_7$).[4] The first CD Cotton effect at 391 nm decreased much more than the second one at 353 nm. The result was a drop of the CD ratio from original values around $R = 1.0$ to remarkably low $R = 0.2$ for thermally denatured notional π-helix $\mathbf{1}^{nH}$ (Figure 5B, bottom). This asymmetric change implied that thermal denaturation caused the transformation into a new thermophilic suprastructure rather than the simple self-disorganization of notional π-helix $\mathbf{1}^{nH}$. Thermal denaturation was irreversible. This irreversibility offered sample decomposition on the structural rather than suprastructural level as alternative but naturally not further explored explanation of the observed changes in the CD spectra at high temperature.

Chemical denaturation of notional π-helix $\mathbf{1}^{nH}$ was explored with guanidinium chloride (GuCl). A rapid decrease with increasing denaturant concentration saturating at $A = -15\,\mathrm{M^{-1}cm^{-1}}$ was observed (Figure 5D). Considering possibly incomplete self-organization without denaturant, a self-organization energy $-\Delta G^{H_2O} \leq 1.3\,\mathrm{kcal\,mol^{-1}}$ was calculated. For comparison, protein denaturation under identical conditions occurs within $-\Delta G^{H_2O} = 5$–$15\,\mathrm{kcal\,mol^{-1}}$.[44,45] In contrast to thermal denaturation, the CD ratio $R \approx 1$ did not change with decreasing CD amplitude during chemical denaturation.

The CD spectrum of notional π-helix $\mathbf{1}^{nH}$ was independent of presence or absence of lipid-bilayer membranes (Figure 5E). Partitioning and eventual suprastructural conformational changes upon binding to bilayer membranes were therefore not detectable by this method.

The CD amplitude decreases with decreasing angle between the exciton-coupled transition moments, from a maximum around 70° to CD silence for parallel transition moments (Figure 6A).[42] The helix–barrel transition during the ligand-gated opening of ion channel $\mathbf{1}^{n}\cdot\mathbf{2}^{m}$ should, therefore, be characterized by CD silencing (Figure 1). This CD silencing was observed during the formation of the purple charge-transfer complex $\mathbf{1}^{n}\cdot\mathbf{2}^{m}$ (Figure 6A; the band-I absorption was practically not affected by the appearance of the weak and very broad charge-transfer band between 500 and 650 nm). The CD amplitude decreased to $A = -8\,\mathrm{M^{-1}cm^{-1}}$, an unprecedented value clearly below the one found for both chemical and thermal denaturation (Figure 5F and 6B, ●). This comparison with denaturation experiments corroborated that the increase in average distance between NDI chromophores by DAN intercalation was likely to contribute to but unlikely to fully account for such a dramatic CD silencing. The increase in CD ratio from $R \approx 1$ to $R = 2.3$ confirmed that a conformational change of the exciton-coupled NDIs occurred (Figure 5F). The decrease in CD amplitude caused by this conformational change was in excellent support of the untwisting motion of the NDI stacks in the notional π-helix $\mathbf{1}^{nH}$ during the ligand-gated opening into barrel-stave ion channel $\mathbf{1}^{n}\cdot\mathbf{2}^{m}$ (Figure 1).

The excimer emission of membrane-bound ligand **2** (Figure 4) decreased during the formation of complex $\mathbf{1}^{n}\cdot\mathbf{2}^{m}$ (Figure 6B). This decrease was consistent with the separation of the (excited) dimers $\mathbf{2}^{2}$ during the intercalation into notional π-helix $\mathbf{1}^{nH}$. Both trends, that is, silencing of the exciton-coupled CD of the NDIs and excimer emission of the DANs, were combined to obtain a Job plot of complex $\mathbf{1}^{n}\cdot\mathbf{2}^{m}$. The effective mole fraction $x_{50} \approx 0.66$ was compatible

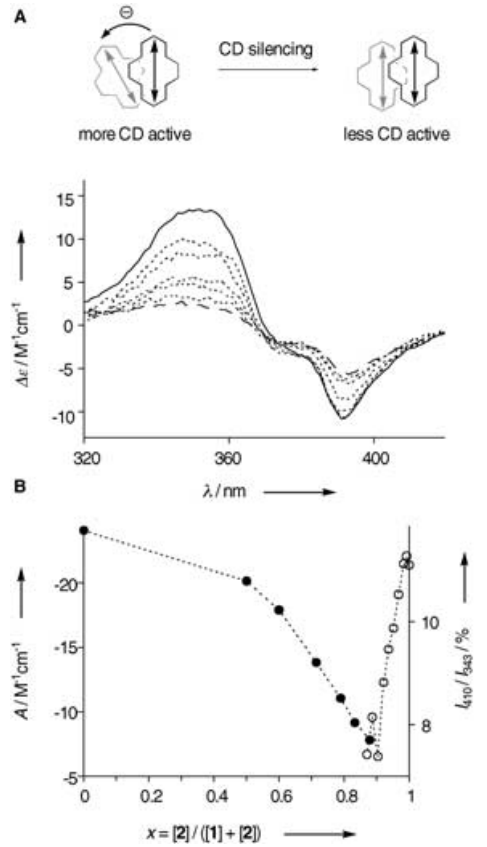

Figure 6. A) CD spectra of **1** (5 μM) in EYPC LUVs with increasing concentration of **2** [0 (——) → 36 μM (-----)]. B) CD amplitude of **1** (●) and fluorescence emission I_{410}/I_{343} of **2** (○) in EYPC LUVs with increasing relative concentrations of **2** and **1**, respectively (10 mM HEPES, 100 mM NaCl, pH 7.9, 25 °C, 200 μM EYPC).

with an onset of helix–barrel transition with 1–3 ligands per rods as in notional ion channel $\mathbf{1}^{n}\cdot\mathbf{2}^{3n}$. Helix–barrel transition around 1–3 ligands per rods matched channel opening by $n = 6.5$ ligands per notional tetrameric π-helix $\mathbf{1}^{4H}$ reasonably well,[36] particularly since ligands **2** may exist as dimers in bilayer membranes (i.e., $n \approx 13$).[43]

The maximal mole fraction $x_{max} \approx 0.9$ suggested that full loading with seven ligands per rod is possible. Geometry-minimized molecular models of the original tetramers $\mathbf{1}^{4}\cdot\mathbf{2}^{12}$ and higher tetramers $\mathbf{1}^{4}\cdot\mathbf{2}^{16}$ and $\mathbf{1}^{4}\cdot\mathbf{2}^{28}$ confirmed that excessive ligand intercalation is conceivable (Figure 3). However, increasing hoop–stave mismatch upon excessive intercalation accounted for an increasing disorder in the overloaded $\mathbf{1}^{4}\cdot\mathbf{2}^{28}$, with some ligands being expelled from the π-stack during optimization. The total length of the π-barrels $\mathbf{1}^{n}\cdot\mathbf{2}^{m}$ naturally increased with increasing number of intercalators, whereas the inner diameter decreased. The fully loaded tetramer $\mathbf{1}^{4}\cdot\mathbf{2}^{28}$ was not hollow anymore. Molecular modeling, therefore, suggested that ion channels $\mathbf{1}^{n}\cdot\mathbf{2}^{m}$ that are open at intermediate ligand intercalation may close in response to an overdose.

Internal decrowding: To probe the relevance of internal crowding for the design of ligand-gated ion channel $\mathbf{1}^{n}\cdot\mathbf{2}^{m}$, control rod **1a** with a truncated methylamine tail was synthesized in 15 steps (Scheme 1, and Supporting Information for Experimental Section): The transformation of diprotected diaminopropionic acid **3** into amide **4** followed by Z deprotection gave amine **5**. As for the original functional rod **1**,[36] anhydride **6** was then treated with amines **5** and **7** to give the asymmetric NDI **8**. Removal of the Z group gave amine **9**, which was coupled with the carboxylic acids along the scaffold of rigid rod **10** and Boc-deprotected to afford the target molecule **1a**.

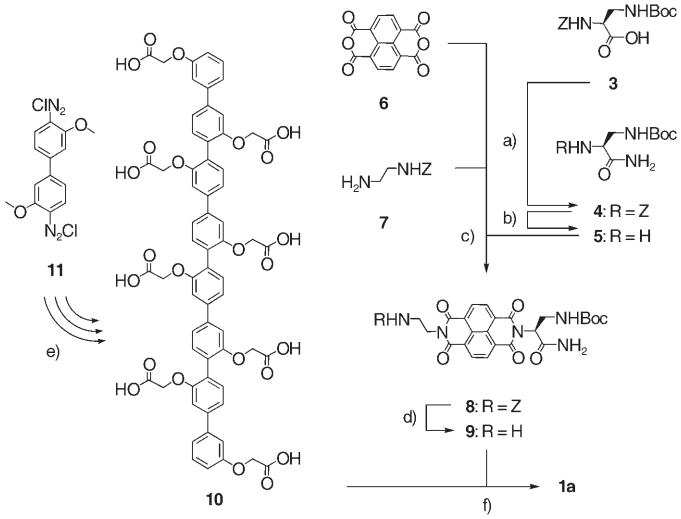

Scheme 1. a) Boc_2O, NH_4HCO_3, MeCN, pyridine, 16 h, RT, 96%; b) H_2, $Pd(OH)_2$/C, MeOH, 6 h, RT, 89%; c) triethylamine, DMF, 48 h, 40 °C, 50%; d) H_2, $Pd(OH)_2$/C, MeOH, 6 h, RT, 90%; e) see ref. [5]; f) 1) HATU, DMF, 2,6-di-*tert*-butyl pyridine, 24 h, RT, 28%; 2) TFA/CH_2Cl_2 1:1, 75%.

In the HPTS assay, ligand gating of ion channel $\mathbf{1}^{n}\cdot\mathbf{2}^{m}$ was demonstrated following the collapse of an applied pH gradient by the change in emission of the intravesiclar, pH-sensitive 8-hydroxypyrene-1,3,6-trisulfonate probe in the presence of **1**, **2** and both. Nearly no activity was observed for **1** without **2** (Figure 7A, d) and **2** without **1** (Figure 7A, e), whereas **1** and **2** together exhibited significant synergistic activity (Figure 7A, a).[36] Ligand **2** failed to activate control rod **1a** (Figure 7A, c) under identical conditions (Figure 7A, b) and at higher concentrations (not shown).

Structural support for ligand gating by a helix–barrel transition from notional π-helix $\mathbf{1}^{nH}$ to notional π-barrel $\mathbf{1}^{n}\cdot\mathbf{2}^{m}$ was obtained from the disappearance of the exciton chirality of twisted π-stacks of self-organized rod **1** upon addition of ligand **2** (Figure 6A). In striking contrast, control rod **1a** with very similar monomer structure was nearly CD silent (Figure 7B).

Taken together, internal decrowding of the notional rigid-rod π-stack architecture $\mathbf{1}^{nH}$ and $\mathbf{1}^{n}\cdot\mathbf{2}^{m}$ resulted in the poor activity expected for the contraction into dimeric complexes $\mathbf{1a}^{2}$ without internal space and helicity. The differences in structure and function were striking considering the similar

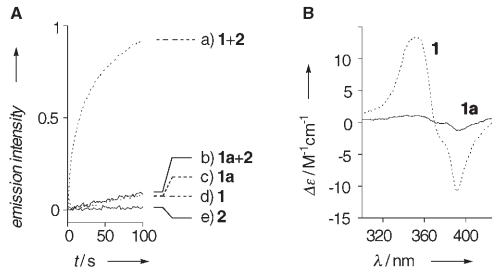

Figure 7. Comparison of A) function and B) suprastructure of **1** and **1a**. (A) Fractional HPTS emission I (λ_{ex} 450 nm, λ_{em} 510 nm) as a function of time after addition of base (ΔpH 0.9) followed by **2** (a, b, e: 20 μM, c, d: 0 μM) and then **1** (a, d: 1.6 μM, from ref. [36]) or **1a** (b, c: 3.2 μM) at $t=0$ s to EYPC–LUVs ⊃ HPTS (10 mM HEPES, 100 mM NaCl, pH 7.0; up to 100 μM **2** did not significantly increase the activity of **1a**+**2** in b). B) CD spectrum of **1** (•••••) and **1a** (——; 10 μM each, 10 mM HEPES, 100 mM NaCl, pH 7.9, 25 °C, 200 μM EYPC).

monomer structure of *p*-octiphenyls **1** and **1a**. They can be interpreted as support for the importance of internal crowding for the design of higher hollow barrel-stave architecture. Molecular models were in agreement with this interpretation.

Conclusion

A colorful, surprisingly detailed and remarkably consistent portrait of a ligand-gated ion channel emerges from a rich collection of experimental facts on functional rigid-rod π-stack architecture, made from scratch. All the characteristics observed in spherical or planar lipid-bilayer membranes by using fluorescent probes or conductance measurements were significant and as planned. Ligand gating was found to be highly cooperative as well as extremely selective, that is, minor changes in both ligand and channel structure cleanly canceled all function. The open ion channels were small, long-lived, surprisingly homogenous, ohmic, and anion selective.

In research focusing on the design of function, it is most important to obtain the experimental evidence for the desired function. However, structural insights on at least the two key concepts of the introduced design strategy appeared desirable (as long as they could be secured under conditions relevant for function). Because of their purple color, presence of charge-transfer complexes in open ion channels was readily detectable with the naked eye. Direct experimental support for the otherwise more elusive helix–barrel transition as structural basis of ligand gating was obtained based on the principles of the exciton chirality method.[42] Corroborated by a series of control experiments, CD silencing by an untwisting rotation of coupled NDI chromophores was in excellent agreement with the conformational change from a CD-active π-helix to a CD-silent barrel-stave ion channel. Because the most stable suprastructure detected in structural studies does not have to (and often does not) correspond to the one responsible for function,[43] we reiterate that the excellent agreement found between functional and structural studies (under meaningful conditions) is remarkable and must be appreciated with appropriate reservation.

Acknowledgements

We thank D. Jeannerat, A. Pinto and J.-P. Saulnier for NMR measurements, P. Perrottet and the group of F. Gülaçar for MS measurements, H. Eder for elemental analyses, and the Swiss NSF for financial support (including the National Research Program "Supramolecular Functional Materials" 4047–057496).

[1] I. Tabushi, Y. Kuroda, K. Yokota, *Tetrahedron Lett.* **1982**, *23*, 4601–4604.
[2] Y. Tanaka, Y. Kobuke, M. Sokabe, *Angew. Chem.* **1995**, *107*, 717–719; *Angew. Chem. Int. Ed. Engl.* **1995**, *34*, 693–694.
[3] T. M. Fyles, D. Loock, X. Zhou, *J. Am. Chem. Soc.* **1998**, *120*, 2997–3003.
[4] N. Sakai, B. Baumeister, S. Matile, *ChemBioChem* **2000**, *1*, 123–125.
[5] B. Baumeister, N. Sakai, S. Matile, *Org. Lett.* **2001**, *3*, 4229–4232.
[6] G. Das, P. Talukdar, S. Matile, *Science* **2002**, *298*, 1600–1602.
[7] V. Gorteau, F. Perret, G. Bollot, J. Mareda, A, N. Lazar, A. W. Coleman, D.-H. Tran, N. Sakai, S. Matile, *J. Am. Chem. Soc.* **2004**, *126*, 13592–13593.
[8] N. Sakai, J. Mareda, S. Matile, *Acc. Chem. Res.* **2005**, *38*, 79–87.
[9] N. Sakai, S. Matile, *Chem. Commun.* **2003**, 2514–2523.
[10] S. Matile, *Chem. Soc. Rev.* **2001**, *30*, 158–167.
[11] R. S. Hector, M. S. Gin, *Supramol. Chem.* **2005**, *17*, 129–134.
[12] S. Matile, A. Som, N. Sordé, *Tetrahedron* **2004**, *60*, 6405–6435.
[13] Y. J. Jeon, H. Kim, S. Jon, N. Selvapalam, D. H. Oh, I. Seo, C.-S. Park, S. R. Jung, D.-S. Koh, K. Kim, *J. Am. Chem. Soc.* **2004**, *126*, 15944–15945.
[14] *Synthetic Ion Channels* (Ed.: U. Koert), *Bioorg. Med. Chem.* **2004**, *12*, 1277–1350, whole Issue.
[15] J. Zhang, B. Jing, S. L. Regen, *J. Am. Chem. Soc.* **2003**, *125*, 13984–13987.
[16] J. M. Boon, B. D. Smith, *Curr. Opin. Chem. Biol.* **2002**, *6*, 749–756.
[17] G. W. Gokel, A. Mukhopadhyay, *Chem. Soc. Rev.* **2001**, *30*, 274–286.
[18] G. J. Kirkovits, C. D. Hall, *Adv. Supramol. Chem.* **2000**, *7*, 1–47.
[19] P. Scrimin, P. Tecilla, *Curr. Opin. Chem. Biol.* **1999**, *3*, 730–735.
[20] H. Bayley, P. S. Cremer, *Nature* **2001**, *413*, 226–230.
[21] S. Terrettaz, W.-P. Ulrich, R. Guerrini, A. Verdini, H. Vogel, *Angew. Chem.* **2001**, *113*, 1790–1793; *Angew. Chem. Int. Ed.* **2001**, *40*, 1740–1743.
[22] D. W. Deamer, D. Branton, *Acc. Chem. Res.* **2002**, *35*, 817–825.
[23] R. S. Lokey, B. L. Iverson, *Nature* **1995**, *375*, 303–305.
[24] G. J. Gabriel, B. L. Iverson, *J. Am. Chem. Soc.* **2002**, *124*, 15174–15175.
[25] J. Lee, V. Guelev, S. Sorey, D. W. Hoffman, B. L. Iverson, *J. Am. Chem. Soc.* **2004**, *126*, 14036–14042.
[26] S. A. Vignon, T. Jarrosson, T. Iijima, H.-R. Tseng, J. M. K. Sanders, J. F. Stoddart, *J. Am. Chem. Soc.* **2004**, *126*, 9884–9885.
[27] T. Iijima, S. A. Vignon, H. R. Tseng, T. Jarrosson, J. M. K. Sanders, F. Marchioni, M. Venturi, E. Apostoli, V. Balzani, J. F. Stoddart, *Chem. Eur. J.* **2004**, *10*, 6375–6392.
[28] D. G. Hamilton, N. Feeder, S. J. Teat, J. M. K. Sanders, *New J. Chem.* **1998**, *22*, 1019–1021.
[29] R. L. Furlan, S. Otto, J. K. M. Sanders, *Proc. Natl. Acad. Sci. USA* **2002**, *99*, 4801–4804.
[30] G. D. Fallon, M. A.-P. Lee, S. J. Langford, P. J. Nichols, *Org. Lett.* **2004**, *6*, 655–658.
[31] M. S. Cubberley, B. L. Iverson, *J. Am. Chem. Soc.* **2001**, *123*, 7560–7563.
[32] F. Würthner, B. Hanke, M. Lysetska, G. Lambright, G. S. Harms, *Org. Lett.* **2005**, *7*, 967–970.

[33] K. Sugiyasu, N. Fujita, S. Shinkai, *Angew. Chem.* **2004**, *116*, 1249–1252; *Angew. Chem. Int. Ed.* **2004**, *43*, 1229–1233.
[34] W. Zhang, D. Horoszewski, J. Decatur, C. Nuckolls, *J. Am. Chem. Soc.* **2003**, *125*, 4870–4873.
[35] B. Baumeister, A. Som, G. Das, N. Sakai, F. Vilbois, D. Gerard, S. P. Shahi, S. Matile, *Helv. Chim. Acta* **2002**, *85*, 2740–2753.
[36] P. Talukdar, G. Bollot, J. Mareda, N. Sakai, S. Matile, *J. Am. Chem. Soc.* **2005**, *127*, 6528–6529.
[37] B. Hille, *Ionic Channels of Excitable Membrane*, 2nd ed., Sinauer Associate, Sunderland, MA, **1992**.
[38] O. S. Smart, J. Breed, G. R. Smith, M. S. P. Sansom, *Biophys. J.* **1997**, *72*, 1109–1126.
[39] J. Gawronski, M. Brzostowska, K. Kacprzak, H. Kolbon, P. Skowronek, *Chirality* **2000**, *12*, 263–268.
[40] J. Reichwagen, H. Hopf, A. Del Guerzo, J. P. Desvergne, H. Bouas-Laurent, *Org. Lett.* **2004**, *6*, 1899–1902.
[41] S. H. White, W. C. Wimley, A. S. Ladokhin, K. Hristova, *Methods Enzymol.* **1998**, *295*, 62–87.
[42] K. Nakanishi, N. Berova, *The Exciton Chirality Method. In Circular Dichroism—Principles and Applications* (Eds: K. Nakanishi, N. Berova, R. W. Woody), VCH, Weinheim, Germany, **1994**, 361–398.
[43] S. Litvinchuk, G. Bollot, J. Mareda, A. Som, D. Ronan, M. R. Shah, P. Perrottet, N. Sakai, S. Matile, *J. Am. Chem. Soc.* **2004**, *126*, 10067–10075.
[44] F. Ahmad, C. C. Bigelow, *J. Biol. Chem.* **1982**, *257*, 12935–12938.
[45] G. Das, S. Matile, *Chirality* **2001**, *13*, 170–176.

Received: May 9, 2005
Published online: August 24, 2005

